

Point Cloud Self-supervised Learning via 3D to Multi-view Masked Autoencoder

Zhimin Chen¹, Yingwei Li², Longlong Jing³, Liang Yang³, Bing Li¹

¹Clemson University ²Johns Hopkins University ³The City University of New York

Abstract

In recent years, the field of 3D self-supervised learning has witnessed significant progress, resulting in the emergence of Multi-Modality Masked AutoEncoders (MAE) methods that leverage both 2D images and 3D point clouds for pre-training. However, a notable limitation of these approaches is that they do not fully utilize the multi-view attributes inherent in 3D point clouds, which is crucial for a deeper understanding of 3D structures. Building upon this insight, we introduce a novel approach employing a 3D to multi-view masked autoencoder to fully harness the multi-modal attributes of 3D point clouds. To be specific, our method uses the encoded tokens from 3D masked point clouds to generate original point clouds and multi-view depth images across various poses. This approach not only enriches the model’s comprehension of geometric structures but also leverages the inherent multi-modal properties of point clouds. Our experiments illustrate the effectiveness of the proposed method for different tasks and under different settings. Remarkably, our method outperforms state-of-the-art counterparts by a large margin in a variety of downstream tasks, including 3D object classification, few-shot learning, part segmentation, and 3D object detection. Code will be available at: <https://github.com/Zhimin-C/Multiview-MAE>

1. Introduction

Three-dimensional (3D) vision has become a critical research topic in applications such as autonomous driving, mixed reality, and robotics due to its ability to understand the human world. However, manually collecting and annotating 3D point cloud data is expensive and time-consuming, making it challenging to develop effective 3D models. Therefore, learning 3D representations in a self-supervised manner has become a core research question.

Some current works investigated self-supervised contrastive learning for point cloud understanding [9, 26, 39, 48]. Recently, inspired by the significantly advanced natural language processing and computer vision area achieved

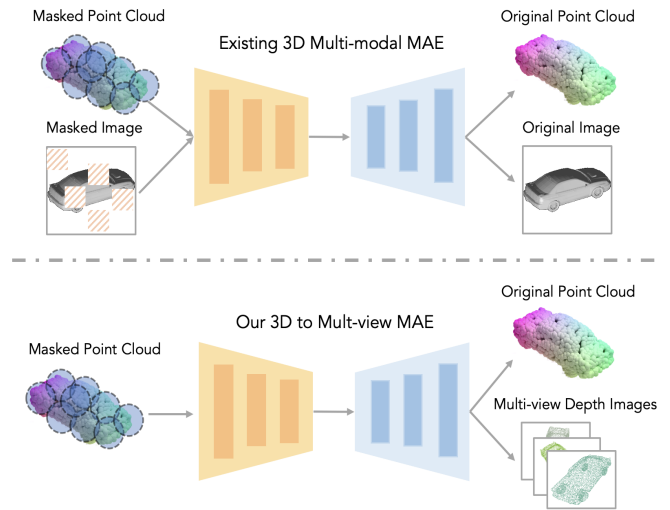


Figure 1. Comparison between our Multiview-MAE and previous multi-modal MAE methods. Previous 3D Multi-modal MAE methods [4, 20] utilize both masked points and corresponding single image as input to reconstruct original point clouds and image. However, this ignores the inherent multi-view attributes of point clouds. In this work, we leverage masked point clouds only to reconstruct original point clouds and **multiple multi-view** depth images at the same time, which makes the 3D network understand pose information and leverages the benefits of rich perceptual features of multi-view projections.

by the masked autoencoder [2, 13, 24], Point-BERT [62], Point-MAE [38], and Point-M2AE [63] have been proposed for 3D reconstruction and achieved state-of-the-art (SOTA) performance on 3D objection classification, part-segmentation, and 3D objection detection tasks. However, these methods rely on 3D data alone, overlooking the valuable correlations that exist within the 2D modality. To solve this problem, recent works like Joint-MAE [20], PiMAE [4], and TAP [56] are proposed to leverage 2D images, thereby augmenting 3D representation learning. However, these models rely on the availability of the corresponding 2D images for pre-training, which limits their generality. Additionally, The PiMAE and Joint-MAE leverage the masked point and masked image to reconstruct the original

point clouds and images. The TAP only reconstructs one image view at a time. Those methods do not take into account the inherent multi-view 2D properties of the 3D data. Previous studies [21, 22, 47, 51] have demonstrated the advantages of exploiting rich perceptual features derived from multi-view projections of point clouds.

In this work, we introduce a novel 3D to multi-view masked autoencoder method named Multiview-MAE to understand multi-view 2D information in 3D point clouds, thereby enhancing 3D representation learning. As shown in Fig 1, our approach diverges from previous 3D multi-modality MAE techniques [4, 20] in two key ways. Firstly, unlike previous methods that require both masked images and point clouds as input, our approach exclusively utilizes masked point clouds. Point clouds inherently encompass multi-modal information, as they can be directly projected into corresponding depth images or rendered as images. Therefore, there is no need for input images for 2D reconstruction purposes. Secondly, instead of reconstructing a single image as in previous methods, we randomly select multiple poses and task the network with reconstructing corresponding multiple-depth images simultaneously. This approach empowers the network to capture multi-view and pose information, which is crucial for 3D representation learning. This holistic methodology enables us to fully exploit the multi-view information inherent in 3D data, resulting in enhanced representation capabilities that encompass geometric knowledge and 2D perspective information.

To demonstrate the generality of our approach, we evaluated the Multiview-MAE on multiple downstream tasks. In shape classification tasks, our method outperforms the baseline Point-MAE [38] method by 2.92%, 3.79%, and 2.05% in the OBJ-BG, OBJ-ONLY, and PB-T50-RS settings of the ScanObjectNN [52] dataset. In the object detection task, our method achieves 64.0 AP₂₅ (+1.9 %) and 42.9 AP₅₀ (+5.0 %) compared to the baseline 3DETR [36] on the ScanNetV2 [11] dataset.

The contributions of our method can be summarized as follows:

1. In this work, We introduce a novel method Multiview-MAE that reconstructs point clouds and generates multiple multi-view depth images directly from masked 3D data. This approach fully leverages inherent multi-view 2D information in point clouds.
2. Our work pioneers the integration of pose information into 3D MAE tasks, harnessing rich perceptual features from multi-view projections to better understand and reconstruct complex 3D structures.
3. Our methods consistently outperform existing approaches across various downstream tasks, emphasizing the critical role of multi-view 2D information within 3D point clouds for effective 3D representation learning.

2. Relative Work

3D Self-Supervised Learning: Many methods have been proposed to learn 3D features from unlabeled 2D data without annotations. Mainstream methods train networks to solve pre-defined pretext tasks. Sauder et al. [49] proposed learning point cloud features by training networks to recognize the relative position of two point cloud segments. Hassani et al. [23] proposed to train networks with multiple pre-defined pretext tasks, including clustering, prediction, and reconstruction for point cloud data. Inspired by the success of contrastive learning in the 2D area, numerous works apply self-supervised contrastive learning in the 3D area [1, 8, 10, 15, 17, 26, 27, 48, 58, 59, 64]. Info3D [48] extend the 2D InfoMax and contrastive learning principles on 3D shapes. PointContrast [58] conducts point-level contrast on two transformed views of the same point clouds. Zhang [64] contrast instances-level representations obtained from the same scenario but processed by different model architectures. As the complementary attributes of point clouds and images, CrossPoint [1] introduces an auxiliary multi-modal contrastive objective that captures 3D-2D correspondence.

Masked Auto-Encoder for Point Cloud: Contrary to contrastive learning methods [5, 6] that learn from pairwise relations, the masked autoencoder aims to reconstruct masked input and learn modality-specific representations. Given the success of MAE in the natural language processing area [13, 43, 44], BEiT [2] proposes to recover the original visual tokens based on the corrupted image patches. MAE [24] directly masks random patches of the input image and reconstructs the missing pixels, which performs great with a high mask ratio. Recently, PointBERT [62] and Point-MAE [38] extend BEiT and MAE from 2D to 3D to reconstruct masked point clouds. The PointM2AE model, as described in Zhang et al. [63], utilizes pyramid architectures in both the encoder and decoder to represent spatial geometries and extract both fine-grained and higher-level semantic features of 3D shapes. However, those methods are only focused on 3D single modalities. Currently, there is limited research exploring the potential of multi-modality masked autoencoders [18, 20, 28]. Recent work joint-MAE [20] and PiMAE [4] proposes 2D-3D joint-MAE frameworks to reconstruct multi-modalities from masked 2D and 3D inputs. However, those works ignore the multi-view attributes of the point cloud, which is crucial for 3D understanding. To bridge this gap, we propose the Multiview-MAE to leverage masked 3D data for multi-view cross-modal generative pre-training and thus enrich the model’s comprehension of point cloud geometric structures and inherent multi-modal properties.

Multimodal Feature Learning: Multimodal feature learning has received increasing attention recently due to the growing availability of multimodal data. It uses complementary information across modalities to improve per-

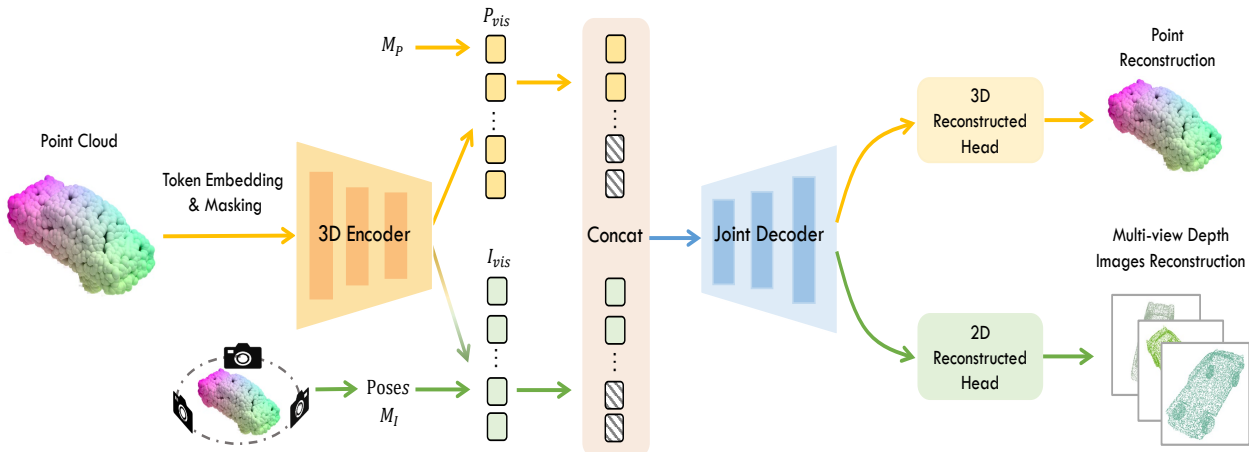


Figure 2. An overview of the Multiview-MAE: Our method innovatively utilizes the multi-view characteristics of 3D point clouds to enhance 3D representation learning. We introduce a novel technique for reconstructing point clouds and multi-view depth images from masked 3D data, uniquely leveraging the inherent multi-view 2D information without depending on corresponding 2D images. Additionally, we are the first to integrate pose information into 3D Masked Autoencoder tasks, enabling the extraction of rich perceptual features from multi-view projections. This approach significantly improves our understanding and reconstruction of complex 3D structures.

formance in downstream tasks. Recent research [1, 12, 27, 37, 45, 59] have shown that pre-training models in a cross-modal learning setting can generate highly transferable representations that effectively improve performance on various downstream tasks. CrossPoint [1] maximizes agreement between point clouds and the corresponding rendered 2D image in the invariant space by contrastive learning. The study by MVTN [21] demonstrates that leveraging multi-view images and the associated correspondences between images and points enhances our understanding of 3D objects. Sautier et al. [50] utilizes superpixels to divide the image and proposes 2D and 3D object-level contrastive loss for 3D pre-training. TAP [56] presents a 3D to 2D generative pre-training technique, building on an established 2D generator. However, the inherent multi-view 2D information for 3D representation learning is still under-explored. In this task, we are at the forefront of investigating how to leverage the inherent multi-view 2D information for boosting 3D representation learning.

3. Method

3.1. Baseline: Point-MAE

Point Patches Generation and Masking: Following Point-BERT [62], the Point-MAE [38] divides the input point cloud into n irregular point patches (may overlap) via Farthest Point Sampling (FPS) and K-Nearest Neighborhood (KNN) algorithm. It utilizes the random masking strategy to mask point clouds with a mask ratio m .

Embedding: To embed each masked point patch, the

Point-MAE method substitutes it with a mask token that is learnable and weighted-shared. Meanwhile, for unmasked point patches (i.e., those that are visible), Point-MAE employs a lightweight PointNet [40] to extract features from the point patches. The visible point patches P^v are hence embedded into visible tokens T^v :

$$T^v = \text{PointNet}(P_v) \quad (1)$$

Backbone: The backbone of Point-MAE is entirely based on standard Transformers, with an asymmetric encoder-decoder. The encoder takes visible tokens T^v as input to generate encoded tokens T^e . In addition, Point-MAE incorporates positional embeddings into each Transformer block, thereby adding location-based information. The decoder is similar to the encoder but contains fewer Transformer blocks. The Point-MAE pads encoded tokens T^e with learnable mask tokens T^m and sends them to the decoder. A complete set of positional embeddings is added to every Transformer block in the decoder part to provide location information to all the tokens. The outputs of the decoder are fed to a simple fully connected (FC) layer to reconstruct the masked 3D coordinates. The encoder-decoder structure is formulated as:

$$T^e = \text{Encoder}(T^v) \quad (2)$$

$$H^m = \text{Decoder}(\text{concat}(T^e, T^m)) \quad (3)$$

The projection head is formulated as:

$$P^{pre} = \text{Reshape}(FC(H^m)) \quad (4)$$

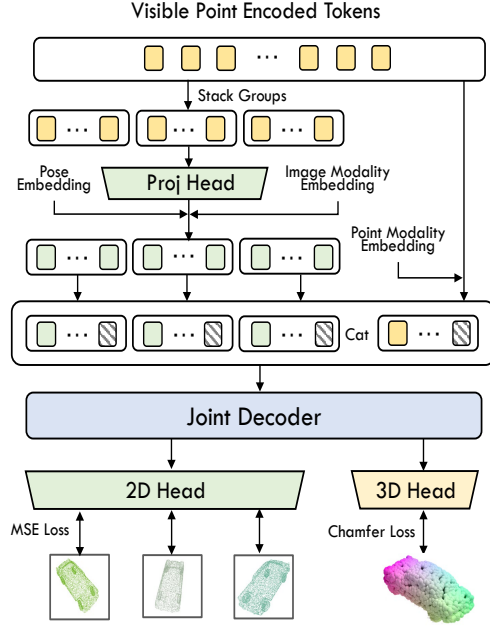


Figure 3. The joint decoder for Multiview-MAE. Encoded visible point tokens are processed by projection heads, projected into multi-view image token positions, and padded to full image token sizes. Those image tokens are concatenated with padded point tokens and sent to the joint decoder to reconstruct point cloud coordinates and complete multi-view 2D depth images obtained from point clouds projection.

Point-MAE’s reconstruction task aims to restore the coordinates of the points in each masked point patch. To evaluate the accuracy of the predicted coordinates of the masked patches, Point-MAE computes the reconstruction loss by l_2 Chamfer Distance [16], which is formulated as:

$$\mathcal{L}_{MAE} = \frac{1}{M_{mask}} \text{Chamfer} (P^{pre}, P^{mask}) \quad (5)$$

where P_{mask} represents the ground truth of masked points.

3.2. 3D to Multi-view Projection and Encoding

Depth Map Projection: To obtain the 2D-3D corresponding relationship, we project the 3D point clouds to multi-view 2D depth images. Then, those depth images are leveraged to guide the 3D to 2D reconstructions. The pytorch3D [46] is utilized to project 3D coordinates to the 2D coordinates. We convert the 2D coordinates to token index by the formulation:

$$\hat{T} = \hat{X}/(H_i/H_t) * H_t + \hat{Y}/(W_i/W_t) \quad (6)$$

Where H_i, W_i represents the height and width of the depth map. H_t, W_t represents the height and width of the 2D token map size. We project 3D coordinates $(X, Y, Z) \in \mathbb{R}^3$ to 2D coordinates $(\hat{X}, \hat{Y}) \in \mathbb{Z}^2$ in a specific view.

Positional Encodings: Following the Point-MAE, our method applies positional encodings to all 3D-related attention layers. For point tokens T_p^v , we utilize a two-layer MLP to encode its corresponding 3D coordinates P_p^v into C_i -channel vectors E_p^p , and element-wisely add them with the token features before feeding into the attention layer. We also add the modality-specific 2-D sinusoidal positional embedding E_p^i to the image tokens T_i^v

Modality Encodings: To let the model understand which token belongs to which modality in the shared decoder part, we add modality-type embeddings E_m^i and E_m^p to the point tokens T_p^v and image tokens T_i^v before sending to the shared decoder. We utilize a two-layer MLP to encode the class of tokens.

Pose Encodings: In the 3D to multi-view masked autoencoder, our method uses masked 3D tokens to reconstruct fully original depth images from different poses. To incorporate the view information into the decoder, we utilize a two-layer MLP to encode the view information of the depth map as the E_v^i and add it to the image tokens before the decoding part. The ablation study for the type of pose for encoding is shown in the *supplementary materials*.

3.3. 3D to Multi-view Masked AutoEncoder

As point clouds include inherent multi-view information, we reconstruct multiple depth images from different poses at the same time. We divide the P^v into different groups $\{P_i^g\}_{i=1}^G$ according to corresponding projected image tokens. G is the number of corresponding image tokens. Then, We utilize the max-pooling and average-pooling to fuse point tokens projected to the same image tokens and utilize the MLP layer to project the fused point features to the image space.

$$I^e = MLP(\text{Stack}(\{Max(P_i^g) + Ave(P_i^g)\}_{i=1}^G)) \quad (7)$$

Then, we pad I^e with trainable masked tokens as I^f and pad visible point tokens T^e with trainable masked tokens as T^f . For the image tokens, we add modality type embedding E_m^i , 2-D sinusoidal positional embedding E_p^i , and projection pose embedding E_v^i before feeding the I^f to the joint decoder. The projection view embedding E_v^i is utilized to inform the decoder that it should reconstruct the depth map from which view. For the point tokens, we add the positional embedding E_p^p and modality type embedding E_m^p before feeding the I^f to the joint decoder.

$$I^f = I^e + E_m^i + E_p^i + E_v^i \quad (8)$$

$$T^f = T^e + E_p^p + E_m^p \quad (9)$$

We concatenate multi-view I^f and T^f to a joint embedding and send them to the joint decoder D_j , which is formulated

Method	[P]	Top-1 Accuracy (%)
PointNet [40]		89.2
PointNet++ [41]		90.5
PointCNN [31]		92.2
SO-Net [29]	✓	92.5
DGCNN [55]		92.9
PCT [19]		93.2
Point Transformer [65]		93.7
Transformer [61]		91.4
Point-BERT [61]	✓	93.2
Point-MAE [38]	✓	93.8
Joint-MAE [20]	✓	94.0
Point-M2AE [63]	✓	94.0
Ours	✓	94.1

Table 1. Shape classification on ModelNet40 [57]. We report the shape classification accuracy (%) on ModelNet40 dataset. [P] represents fine-tuning after self-supervised pre-training.

as:

$$P^d, \{I_i^d\}_{i=1}^K = D_j \left(\text{Concat}(T^f, \{I_i^f\}_{i=1}^K) \right) \quad (10)$$

Where K represents the number of depth map projection views for reconstruction. After that, we utilize the modal-specific projection layer to project 3D and 2D features.

$$P^{pre} = \text{Reshape} (FC (P^d)) \quad (11)$$

$$\{I_i^{pre}\}_{i=1}^K = \text{Reshape} (FC(\{I_i^d\}_{i=1}^K)) \quad (12)$$

Where FC is a fully connected layer.

3.4. Objective Function

We utilize Chamfer Distance loss and MSE loss to reconstruct 3D coordinates and 2D multi-view depth images, formulated as:

$$\mathcal{L}_{3D} = \frac{1}{M_{mask}} \text{Chamfer} (P^{pre}, P^{gt}), \quad (13)$$

$$\mathcal{L}_{2D} = \frac{1}{K} \sum_{i=1}^K \text{MSE} (\mathbf{I}_i^{pre}, \mathbf{I}_i^{gt}) \quad (14)$$

Where P^{gt} represents the set of masked patches and I_i^{gt} represents the projected depth image from view i . Finally, we sum up all three losses as the final loss for our method:

$$L = L_{3D} + L_{2D} \quad (15)$$

After pretraining, we abandon the decoder and only keep the 3D encoders of the downstream tasks. Rendered depth images are not utilized in the downstream fine-tuning stage.

Method	[P]	OBJ-BG	OBJ-ONLY	PB-T50-RS
PointNet [40]		73.3	79.2	68.0
PointNet++ [41]		82.3	84.3	77.9
DGCNN [55]		82.8	86.2	78.1
PointCNN [31]		86.1	85.5	78.5
Transformer [61]		79.86	80.55	77.24
Point-BERT [61]	✓	87.43	88.12	83.07
Point-MAE [38]	✓	90.02	88.29	85.18
Joint-MAE [20]	✓	90.94	88.86	86.07
TAP [56]	✓	90.36	89.50	85.67
Point-M2AE [63]	✓	91.22	88.81	86.43
Ours	✓	92.94	92.08	87.23
<i>Improvement</i>		+2.92	+3.79	+2.05

Table 2. Shape classification on ScanObjectNN [54]. We report the accuracy (%) on the three splits of ScanObjectNN. [P] represents fine-tuning after self-supervised pre-training.

4. Experiments

Due to the page limitation, implementation details of our proposed method and more ablation studies are provided in *supplementary materials*.

Datasets. In our experiments, we use several datasets, including ShapeNet [3], ModelNet40 [57], ScanObjectNN [54], ShapeNetPart dataset [60], and ScanNetV2 dataset [11]. The ShapeNet [3] comprises about 51,300 clean 3D models covering 55 common object categories. The widely adopted ModelNet40 [57] consists of synthetic 3D shapes of 40 categories, of which 9,843 samples are for training and the other 2,468 are for validation. The challenging ScanObjectNN [53] contains 11,416 training and 2,882 validation point clouds of 15 categories, which are captured from the noisy real-world scenes and thus have domain gaps with the pre-trained ShapeNet [3] dataset. ScanObjectNN is divided into three splits for evaluation, OBJ-BG, OBJ-ONLY, and PB-T50-RS, where PB-T50-RS is the most difficult for recognition. ShapeNetPart [60] is a widely used benchmark dataset for semantic segmentation of 3D point clouds, which consists of 16,881 models across 16 categories, including objects such as chairs, tables, lamps, and airplanes. The ScanNet [11] is an indoor scene dataset consisting of 1513 reconstructed meshes, among which 1201 are training samples and 312 are validation samples.

4.1. Self-Supervised Pre-training

Settings: We utilize the ShapeNet [3] for pertaining. To obtain a dense depth map, the input point number N is set as 1024. The number of the projection view K is set to 3 and the depth map size is set as 224×224 . Random scaling and random rotation are implemented as data augmentation

Method	[P]	5-way		10-way	
		10-shot	20-shot	10-shot	20-shot
Transformer [61]		87.8 ± 5.2	93.3 ± 4.3	84.6 ± 5.5	89.4 ± 6.3
Point-BERT [61]	✓	94.6 ± 3.1	96.3 ± 2.7	91.0 ± 5.4	92.7 ± 5.1
Point-MAE [38]	✓	96.3 ± 2.5	97.8 ± 1.8	92.6 ± 4.1	95.0 ± 3.0
Joint-MAE [20]	✓	96.7 ± 2.2	97.9 ± 1.8	92.6 ± 3.7	95.1 ± 2.6
Point-M2AE [63]	✓	96.8 ± 1.8	98.3 ± 1.4	92.3 ± 4.5	95.0 ± 3.0
TAP [56]	✓	97.3 ± 1.8	97.8 ± 1.7	93.1 ± 2.6	95.8 ± 1.0
Ours	✓	97.5 ± 2.1	98.4 ± 1.3	93.4 ± 3.9	96.0 ± 2.1

Table 3. Few-shot classification on ModelNet40 [57]. We report the average accuracy (%) and standard deviation (%) of 10 independent experiments. [P] represents fine-tuning after self-supervised pre-training.

Method	[P]	mIoU _C	mIoU _I
PointNet [40]		80.39	83.70
PointNet++ [41]		81.85	85.10
DGCNN [55]		82.33	85.20
Transformer [61]		83.42	85.10
Point-BERT [61]	✓	84.11	85.60
Point-MAE [38]	✓	-	86.10
Joint-MAE [38]	✓	85.41	86.28
Point-M2AE [63]	✓	84.86	86.51
Ours	✓	85.58	86.57

Table 4. Part segmentation on ShapeNetPart [60]. mIoU_C (%) and mIoU_I (%) denote the mean IoU across all part categories and all instances in the dataset, respectively. [P] represents fine-tuning after self-supervised pre-training.

during pre-training. Our method employs an AdamW optimizer [35] and cosine learning rate decay [34]. The network is trained for 300 epochs with a batch size of 128. The initial learning rate, weight decay, and mask ratio are set to 2×10^{-4} , 0.05, and 0.75.

4.2. Downstream Tasks

For fine-tuning downstream tasks, we abandon the decoder and only keep the 3D encoders.

Shape Classification. We fine-tune the proposed method on ModelNet40 [57] and ScanObjectNN [54] datasets, which contain synthetic objects and real-world instances, respectively. During training in both dataset, we utilize data augmentation techniques such as random scaling and random translation. For the ModelNet40 dataset, we use the standard voting method [33] as Point-BERT for a fair comparison. Like the baseline method Point-MAE, we use 1024 points during training and testing. As shown

Methods	[P]	AP_{25}	AP_{50}
VoteNet [42]		58.6	33.5
PointContrast [58]	✓	59.2	38.0
Hou et al. [25]	✓	-	39.3
4DContrast [7]	✓	-	40.0
DepthContrast [64]	✓	64.0	42.9
DPCo [30]	✓	64.2	41.5
3DETR [36]		62.1	37.9
+Point-BERT[62]	✓	61.0	38.3
+Point-MAE [38]	✓	62.8	40.1
+MaskPoint [32]	✓	63.4	40.6
+ACT [14]	✓	63.5	41.0
+PiMAE [4]	✓	63.1	40.8
+TAP [56]	✓	63.0	41.4
+ Ours	✓	64.0	42.9

Table 5. 3D object detection results on ScanNet dataset. We adopt the average precision with 3D IoU thresholds of 0.25 (AP_{25}) and 0.5 (AP_{50}) for the evaluation metrics. [P] represents fine-tuning after self-supervised pre-training.

in Table 1, in the ModelNet40 dataset, our method achieves an accuracy of 94.1%, which is an improvement of 2.7% compared to training from scratch (91.4%) and surpasses the baseline Point-MAE by 0.3%. This improvement is significant, considering that ModelNet40 is a relatively small dataset. For the ScanObjectNN dataset, we conduct experiments on three variants: OBJ-BG, OBJ-ONLY, and PBT50-RS. As shown in Table 2, our method significantly improves the baseline Point-MAE by 2.92%, 3.79%, and 2.05% for the three variants, respectively. It is important to highlight that our performance also significantly exceeds that of Joint-MAE [20], which employs a multi-modality MAE structure but overlooks the intrinsic multi-view nature of point clouds. This substantial gain underscores the critical

# Pose Pool Size	OBJ-BG	OBJ-ONLY
3	91.17	90.28
6	91.96	91.27
12	92.94	92.08
24	92.61	91.83
36	92.12	91.71

Table 6. Ablation study for the number of pose pool size on the 3D object classification tasks in ScanObjectNN dataset.

importance of harnessing multi-view information in 3D pre-training tasks, demonstrating that exploiting rich perceptual features derived from multi-view projections of point clouds benefits the 3D representation learning and thus can yield considerable improvements in downstream tasks.

Few-shot Learning: We conducted few-shot learning experiments on the ModelNet40 dataset [57] using the n -way, m -shot setting, following the protocol of Point-MAE. During training, we randomly selected n classes and m objects from each class. During testing, we randomly selected 20 unseen objects from each of the n classes for evaluation. We conducted 10 independent experiments for each setting and reported the mean accuracy with standard deviation. The results of our fine-tuned few-shot classification are shown in Table 3. Our method outperformed the baseline and state-of-the-art methods in all settings.

Part Segmentation: We evaluate our method’s representation learning capability on the ShapeNetPart dataset [60], which contains 14,007 and 2,874 samples with 16 object categories and 50 part categories for training and validation. Following Point-MAE [38], we sample 2,048 points from each input instance and adopt the same segmentation head [40, 41] for the fair comparison, which concatenates the output features from different transformer blocks of the encoder. The head only conducts simple upsampling for point tokens at different stages and concatenates them alone with the feature dimension as the output. We report mean IoU (mIoU) for all instances, with IoU for each category. Table 4 indicates that our method improves the baseline method Point-MAE and surpasses the state-of-the-art method Point-M2AE in all settings.

3D Object Detection: To demonstrate the generality of the proposed method, we also pre-train the Multiview-MAE on the indoor ScanNetV2 dataset [11] and subsequently fine-tune our method on the object detection task. Our baseline is 3DETR [36], which consists of a 3-block encoder and a transformer decoder. We utilize the same backbone as 3DETR. The Table 5 indicates that Our method achieves 64.0 AP₂₅ (+1.9) and 42.9 AP₅₀ (+5.0) compared to the baseline 3DETR on the ScanNetV2 [11] dataset. Furthermore, we benchmark our method against PiMAE [4], a novel approach introduced in the CVPR 2023 paper, which

# Reconstructed Views	OBJ-BG	OBJ-ONLY
1	91.30	90.71
2	92.26	91.33
3	92.94	92.08
4	92.21	91.18
5	92.13	91.02

Table 7. Ablation study for the number of reconstructed views on the 3D object classification task in ScanObjectNN dataset.

integrates a multi-modality structure. PiMAE is designed to leverage both masked single RGB images and point clouds for reconstructing the original image and point clouds. Despite PiMAE’s ability to enable point clouds to learn texture information from images, it overlooks the multi-view characteristics of point clouds. Our method’s considerable superiority over PiMAE underscores the critical importance of leveraging multi-view information for effective 3D representation learning. This is particularly pivotal in tasks like 3D object detection, where spatial and geometric awareness is crucial. These experimental results not only demonstrate the effectiveness of our method in enhancing 3D object detection but also highlight its broad applicability across various other 3D tasks. The significant improvements achieved suggest that focusing on the multi-view aspects of point clouds is instrumental in advancing the field of 3D representation learning, opening avenues for further research and development in this domain.

4.3. Ablation Study

The Effectiveness of Poses Pool Size: The pose pool size represents the total number of poses that can be leveraged in our 3D to multi-view MAE method. The ablation study detailed in Table 6 investigates the impact of varying the number of views in the network on 3D object classification performance, using the ScanObjectNN dataset. The study examines a range of views: 3, 6, 12, 24, and 36 to understand how they affect classification accuracy. The results reveal a notable trend: as the number of views increases, there’s generally an improvement in classification accuracy, achieving the best performance at 12 views. Beyond this optimal point, however, the performance decreases with the increase of projected views. This pattern indicates that while increasing the number of views contributes positively to the network’s understanding and representation of 3D objects, there is a point beyond which additional views do not yield further benefits. This is because too many views introduce the redundancy of view-specific information, leading to a slight decrease in the network’s efficiency.

The Effectiveness of Network Reconstructed View Numbers: Our method enhances multi-view understanding by randomly selecting several view poses from the pose

Modality		Joint Decoder	OBJ-BG	OBJ-ONLY
3D	2D			
✓	-	-	90.02	88.29
-	✓	-	92.15	91.22
✓	-	✓	90.36	89.86
-	✓	✓	92.73	91.91
✓	✓	-	92.38	91.64
✓	✓	✓	92.94	92.08

Table 8. Ablation study for the shared decoder and different modality losses on the 3D object classification task in ScanObjectNN dataset.

pool mentioned above, enabling the model to reconstruct corresponding multiple projected depth images. This ablation study focuses on finding the optimal number of reconstructed views for enhancing 3D representation learning in the ScanObjectNN [54] dataset. We examined the impact of the number of reconstructed views from one to five on classification performance in OBJ-BG and OBJ-ONL settings. According to the results in Table 7, accuracy consistently increases with the number of views, peaking at three views. Beyond this point, however, the trend indicates a decrease in performance. This suggests that multiple reconstructed views enhance the network’s understanding of multi-view information. However, too many reconstructed views will make the length of the input sequences processed by the decoder very large, thus impacting the network’s learning efficiency and capacity.

The Effectiveness of Multi-view 2D Reconstruction and the Shared Decoder: The ablation study in Table 8 highlights the significant contribution of our proposed 3D to multi-view MAE in enhancing 3D representation learning, as compared to the baseline Point-MAE [38], which utilizes only the 3D modality and shown in the first line. By directly reconstructing multiple multi-view depth images from masked point clouds, our method already outperforms the Point-MAE by a large margin, which demonstrates the effectiveness of leveraging multi-view information for 3D representation learning. Furthermore, by leveraging the proposed joint decoder, the performance of both Point-MAE and the proposed module is improved. This is because, in the joint decoder, the point cloud’s geometric information and the multi-view information are complementary to each other and thus improve the representation learning. Finally, by combining 3D reconstructing, multi-view depth image reconstruction, and the joint decoder, our framework achieves the best performance, indicating the complementary nature of 3D modality-specific features and multi-view features of point clouds. Our contribution, therefore, lies in the introduction and integration of the multi-view information, which, when combined with the existing 3D modality, significantly enhances the over-

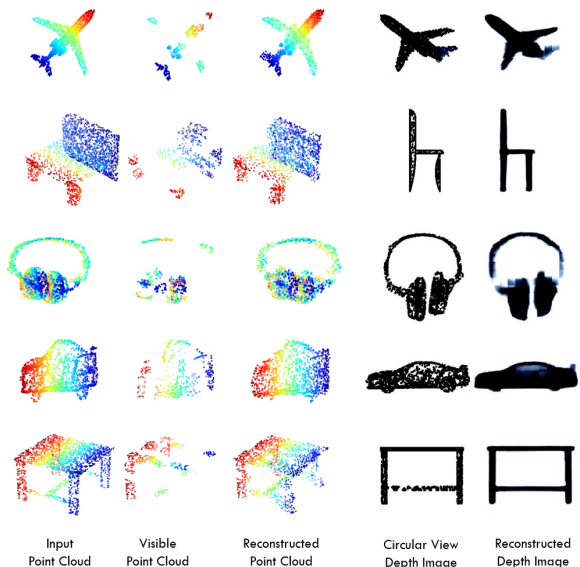


Figure 4. Visualization of 3D to multi-view masked autoencoder. Our method not only can reconstruct point clouds from masked input but also generate multi-view depth images.

all 3D representation learning. This advancement demonstrates the value of incorporating multi-view and pose information into the 3D representation learning framework.

5. Visualization

In Figure 4, to verify the constructed performance of Multiview-MAE, we visualize the input point clouds, the masked point clouds, the reconstructed point clouds, projected depth images, and the reconstructed images, respectively in each row. Our method not only can reconstruct point clouds from masked input but also generate multi-view depth images, demonstrating its ability to capture the intrinsic multi-modality information of point clouds.

6. Conclusion

This paper presented a novel approach for 3D representation learning, introducing a 3D to multi-view Masked AutoEncoder named Multiview-MAE that uses the inherent multi-view attributes of 3D point clouds. Our method diverges from traditional models by exclusively using masked point clouds to reconstruct original point clouds and multiple multi-view depth images, enabling the learning of rich perceptual features from multi-view projections. This strategy effectively leverages the rich multi-view perceptual features and poses information inherent in point clouds, setting our method apart from previous multi-modal MAE methods. Our experiments demonstrate that our proposed method significantly outperforms state-of-the-art 3D self-supervised learning methods on all downstream tasks. These results

underline the advantages of our method in fully exploiting the multi-modality and multi-view properties of 3D data.

References

- [1] Mohamed Afham, Isuru Dissanayake, Dinithi Dissanayake, Amaya Dharmasiri, Kanchana Thilakarathna, and Ranga Rodrigo. Crosspoint: Self-supervised cross-modal contrastive learning for 3d point cloud understanding. In *Proceedings of the IEEE/CVF Conference on Computer Vision and Pattern Recognition*, pages 9902–9912, 2022. 2, 3
- [2] Hangbo Bao, Li Dong, and Furu Wei. Beit: Bert pre-training of image transformers. *arXiv preprint arXiv:2106.08254*, 2021. 1, 2
- [3] Angel X Chang, Thomas Funkhouser, Leonidas Guibas, Pat Hanrahan, Qixing Huang, Zimo Li, Silvio Savarese, Manolis Savva, Shuran Song, Hao Su, et al. Shapenet: An information-rich 3d model repository. *arXiv preprint arXiv:1512.03012*, 2015. 5
- [4] Anthony Chen, Kevin Zhang, Renrui Zhang, Zihan Wang, Yuheng Lu, Yandong Guo, and Shanghang Zhang. Pimae: Point cloud and image interactive masked autoencoders for 3d object detection. In *Proceedings of the IEEE/CVF Conference on Computer Vision and Pattern Recognition*, pages 5291–5301, 2023. 1, 2, 6, 7
- [5] Ting Chen, Simon Kornblith, Mohammad Norouzi, and Geoffrey Hinton. A simple framework for contrastive learning of visual representations. In *International conference on machine learning*, pages 1597–1607. PMLR, 2020. 2
- [6] Xinlei Chen and Kaiming He. Exploring simple siamese representation learning. In *Proceedings of the IEEE/CVF Conference on Computer Vision and Pattern Recognition*, pages 15750–15758, 2021. 2
- [7] Yujin Chen, Matthias Nießner, and Angela Dai. 4dcontrast: Contrastive learning with dynamic correspondences for 3d scene understanding. In *Computer Vision—ECCV 2022: 17th European Conference, Tel Aviv, Israel, October 23–27, 2022, Proceedings, Part XXXII*, pages 543–560. Springer, 2022. 6
- [8] Zhimin Chen and Bing Li. Bridging the domain gap: Self-supervised 3d scene understanding with foundation models. *arXiv preprint arXiv:2305.08776*, 2023. 2
- [9] Zhimin Chen, Longlong Jing, Yang Liang, YingLi Tian, and Bing Li. Multimodal semi-supervised learning for 3d objects. *arXiv preprint arXiv:2110.11601*, 2021. 1
- [10] Zhimin Chen, Longlong Jing, Liang Yang, Yingwei Li, and Bing Li. Class-level confidence based 3d semi-supervised learning. In *Proceedings of the IEEE/CVF Winter Conference on Applications of Computer Vision*, pages 633–642, 2023. 2
- [11] Angela Dai, Angel X Chang, Manolis Savva, Maciej Habber, Thomas Funkhouser, and Matthias Nießner. Scannet: Richly-annotated 3d reconstructions of indoor scenes. In *Proceedings of the IEEE conference on computer vision and pattern recognition*, pages 5828–5839, 2017. 2, 5, 7
- [12] Karan Desai and Justin Johnson. Virtex: Learning visual representations from textual annotations. In *Proceedings of the IEEE/CVF conference on computer vision and pattern recognition*, pages 11162–11173, 2021. 3
- [13] Jacob Devlin, Ming-Wei Chang, Kenton Lee, and Kristina Toutanova. Bert: Pre-training of deep bidirectional transformers for language understanding. *arXiv preprint arXiv:1810.04805*, 2018. 1, 2
- [14] Runpei Dong, Zekun Qi, Linfeng Zhang, Junbo Zhang, Jianjian Sun, Zheng Ge, Li Yi, and Kaisheng Ma. Autoencoders as cross-modal teachers: Can pretrained 2d image transformers help 3d representation learning? *arXiv preprint arXiv:2212.08320*, 2022. 6
- [15] Bi’an Du, Xiang Gao, Wei Hu, and Xin Li. Self-contrastive learning with hard negative sampling for self-supervised point cloud learning. In *Proceedings of the 29th ACM International Conference on Multimedia*, pages 3133–3142, 2021. 2
- [16] Haoqiang Fan, Hao Su, and Leonidas J Guibas. A point set generation network for 3d object reconstruction from a single image. In *Proceedings of the IEEE conference on computer vision and pattern recognition*, pages 605–613, 2017. 4
- [17] Ziyue Feng, Longlong Jing, Peng Yin, Yingli Tian, and Bing Li. Advancing self-supervised monocular depth learning with sparse lidar. In *Conference on Robot Learning*, pages 685–694. PMLR, 2022. 2
- [18] Xinyang Geng, Hao Liu, Lisa Lee, Dale Schuurams, Sergey Levine, and Pieter Abbeel. Multimodal masked autoencoders learn transferable representations. *arXiv preprint arXiv:2205.14204*, 2022. 2
- [19] Meng-Hao Guo, Jun-Xiong Cai, Zheng-Ning Liu, Tai-Jiang Mu, Ralph R Martin, and Shi-Min Hu. Pct: Point cloud transformer. *Computational Visual Media*, 7(2):187–199, 2021. 5
- [20] Ziyu Guo, Xianzhi Li, and Pheng Ann Heng. Joint-mae: 2d-3d joint masked autoencoders for 3d point cloud pre-training. *arXiv preprint arXiv:2302.14007*, 2023. 1, 2, 5, 6
- [21] Abdullah Hamdi, Silvio Giancola, and Bernard Ghanem. Mvtn: Multi-view transformation network for 3d shape recognition. In *Proceedings of the IEEE/CVF International Conference on Computer Vision*, pages 1–11, 2021. 2, 3
- [22] Abdullah Hamdi, Silvio Giancola, and Bernard Ghanem. Voint cloud: Multi-view point cloud representation for 3d understanding. *arXiv preprint arXiv:2111.15363*, 2021. 2
- [23] Kaveh Hassani and Mike Haley. Unsupervised multi-task feature learning on point clouds. In *Proceedings of the IEEE/CVF International Conference on Computer Vision*, pages 8160–8171, 2019. 2
- [24] Kaiming He, Xinlei Chen, Saining Xie, Yanghao Li, Piotr Dollár, and Ross Girshick. Masked autoencoders are scalable vision learners. In *Proceedings of the IEEE/CVF Conference on Computer Vision and Pattern Recognition*, pages 16000–16009, 2022. 1, 2
- [25] Ji Hou, Benjamin Graham, Matthias Nießner, and Saining Xie. Exploring data-efficient 3d scene understanding with contrastive scene contexts. In *Proceedings of the IEEE/CVF Conference on Computer Vision and Pattern Recognition*, pages 15587–15597, 2021. 6
- [26] Siyuan Huang, Yichen Xie, Song-Chun Zhu, and Yixin Zhu. Spatio-temporal self-supervised representation learning for 3d point clouds. In *Proceedings of the IEEE/CVF Inter-*

- national Conference on Computer Vision*, pages 6535–6545, 2021. 1, 2
- [27] Longlong Jing, Yucheng Chen, Ling Zhang, Mingyi He, and Yingli Tian. Self-supervised modal and view invariant feature learning. *arXiv preprint arXiv:2005.14169*, 2020. 2, 3
- [28] Gukyeong Kwon, Zhaowei Cai, Avinash Ravichandran, Erhan Bas, Rahul Bhotika, and Stefano Soatto. Masked vision and language modeling for multi-modal representation learning. *arXiv preprint arXiv:2208.02131*, 2022. 2
- [29] Jiaxin Li, Ben M Chen, and Gim Hee Lee. So-net: Self-organizing network for point cloud analysis. In *Proceedings of the IEEE conference on computer vision and pattern recognition*, pages 9397–9406, 2018. 5
- [30] Lanxiao Li and Michael Heizmann. A closer look at invariances in self-supervised pre-training for 3d vision. In *Computer Vision–ECCV 2022: 17th European Conference, Tel Aviv, Israel, October 23–27, 2022, Proceedings, Part XXX*, pages 656–673. Springer, 2022. 6
- [31] Yangyan Li, Rui Bu, Mingchao Sun, Wei Wu, Xinhan Di, and Baoquan Chen. Pointcnn: Convolution on x-transformed points. *Advances in neural information processing systems*, 31, 2018. 5
- [32] Haotian Liu, Mu Cai, and Yong Jae Lee. Masked discrimination for self-supervised learning on point clouds. *arXiv preprint arXiv:2203.11183*, 2022. 6
- [33] Yongcheng Liu, Bin Fan, Shiming Xiang, and Chunhong Pan. Relation-shape convolutional neural network for point cloud analysis. In *Proceedings of the IEEE/CVF conference on computer vision and pattern recognition*, pages 8895–8904, 2019. 6
- [34] Ilya Loshchilov and Frank Hutter. Sgdr: Stochastic gradient descent with warm restarts. *arXiv preprint arXiv:1608.03983*, 2016. 6
- [35] Ilya Loshchilov and Frank Hutter. Decoupled weight decay regularization. *arXiv preprint arXiv:1711.05101*, 2017. 6
- [36] Ishan Misra, Rohit Girdhar, and Armand Joulin. An end-to-end transformer model for 3d object detection. In *Proceedings of the IEEE/CVF International Conference on Computer Vision*, pages 2906–2917, 2021. 2, 6, 7
- [37] Pedro Morgado, Nuno Vasconcelos, and Ishan Misra. Audio-visual instance discrimination with cross-modal agreement. In *Proceedings of the IEEE/CVF Conference on Computer Vision and Pattern Recognition*, pages 12475–12486, 2021. 3
- [38] Yatian Pang, Wenxiao Wang, Francis EH Tay, Wei Liu, Yonghong Tian, and Li Yuan. Masked autoencoders for point cloud self-supervised learning. *arXiv preprint arXiv:2203.06604*, 2022. 1, 2, 3, 5, 6, 7, 8
- [39] Omid Poursaeed, Tianxing Jiang, Han Qiao, Nayun Xu, and Vladimir G Kim. Self-supervised learning of point clouds via orientation estimation. In *2020 International Conference on 3D Vision (3DV)*, pages 1018–1028. IEEE, 2020. 1
- [40] Charles R Qi, Hao Su, Kaichun Mo, and Leonidas J Guibas. Pointnet: Deep learning on point sets for 3d classification and segmentation. In *Proceedings of the IEEE conference on computer vision and pattern recognition*, pages 652–660, 2017. 3, 5, 6, 7
- [41] Charles Ruizhongtai Qi, Li Yi, Hao Su, and Leonidas J Guibas. Pointnet++: Deep hierarchical feature learning on point sets in a metric space. *Advances in neural information processing systems*, 30, 2017. 5, 6, 7
- [42] Charles R Qi, Or Litany, Kaiming He, and Leonidas J Guibas. Deep hough voting for 3d object detection in point clouds. In *proceedings of the IEEE/CVF International Conference on Computer Vision*, pages 9277–9286, 2019. 6
- [43] Alec Radford, Karthik Narasimhan, Tim Salimans, Ilya Sutskever, et al. Improving language understanding by generative pre-training. In *Proceedings of the 2019 3rd International Conference on Natural Language Processing and Information Retrieval*. Association for Computing MachineryNew YorkNYUnited States, 2019. 2
- [44] Alec Radford, Jeffrey Wu, Rewon Child, David Luan, Dario Amodei, Ilya Sutskever, et al. Language models are unsupervised multitask learners. *OpenAI blog*, 1(8):9, 2019. 2
- [45] Alec Radford, Jong Wook Kim, Chris Hallacy, Aditya Ramesh, Gabriel Goh, Sandhini Agarwal, Girish Sastry, Amanda Askell, Pamela Mishkin, Jack Clark, et al. Learning transferable visual models from natural language supervision. In *International conference on machine learning*, pages 8748–8763. PMLR, 2021. 3
- [46] Nikhila Ravi, Jeremy Reizenstein, David Novotny, Taylor Gordon, Wan-Yen Lo, Justin Johnson, and Georgia Gkioxari. Accelerating 3d deep learning with pytorch3d. *arXiv:2007.08501*, 2020. 4
- [47] Damien Robert, Bruno Vallet, and Loic Landrieu. Learning multi-view aggregation in the wild for large-scale 3d semantic segmentation. In *Proceedings of the IEEE/CVF Conference on Computer Vision and Pattern Recognition*, pages 5575–5584, 2022. 2
- [48] Aditya Sanghi. Info3d: Representation learning on 3d objects using mutual information maximization and contrastive learning. In *European Conference on Computer Vision*, pages 626–642. Springer, 2020. 1, 2
- [49] Jonathan Sauder and Bjarne Sievers. Self-supervised deep learning on point clouds by reconstructing space. *Advances in Neural Information Processing Systems*, 32, 2019. 2
- [50] Corentin Sautier, Gilles Puy, Spyros Gidaris, Alexandre Boulch, Andrei Bursuc, and Renaud Marlet. Image-to-lidar self-supervised distillation for autonomous driving data. In *Proceedings of the IEEE/CVF Conference on Computer Vision and Pattern Recognition*, pages 9891–9901, 2022. 3
- [51] Hang Su, Subhansu Maji, Evangelos Kalogerakis, and Erik Learned-Miller. Multi-view convolutional neural networks for 3d shape recognition. In *Proceedings of the IEEE international conference on computer vision*, pages 945–953, 2015. 2
- [52] Mikaela Angelina Uy, Quang-Hieu Pham, Binh-Son Hua, Duc Thanh Nguyen, and Sai-Kit Yeung. Revisiting point cloud classification: A new benchmark dataset and classification model on real-world data. In *International Conference on Computer Vision (ICCV)*, 2019. 2
- [53] Mikaela Angelina Uy, Quang-Hieu Pham, Binh-Son Hua, Thanh Nguyen, and Sai-Kit Yeung. Revisiting point cloud classification: A new benchmark dataset and classification

- model on real-world data. In *Proceedings of the IEEE/CVF International Conference on Computer Vision*, pages 1588–1597, 2019. [5](#)
- [54] Mikaela Angelina Uy, Quang-Hieu Pham, Binh-Son Hua, Thanh Nguyen, and Sai-Kit Yeung. Revisiting point cloud classification: A new benchmark dataset and classification model on real-world data. In *Proceedings of the IEEE/CVF international conference on computer vision*, pages 1588–1597, 2019. [5](#), [6](#), [8](#)
- [55] Yue Wang, Yongbin Sun, Ziwei Liu, Sanjay E Sarma, Michael M Bronstein, and Justin M Solomon. Dynamic graph cnn for learning on point clouds. *Acm Transactions On Graphics (tog)*, 38(5):1–12, 2019. [5](#), [6](#)
- [56] Ziyi Wang, Xumin Yu, Yongming Rao, Jie Zhou, and Jiwen Lu. Take-a-photo: 3d-to-2d generative pre-training of point cloud models. In *Proceedings of the IEEE/CVF International Conference on Computer Vision*, pages 5640–5650, 2023. [1](#), [3](#), [5](#), [6](#)
- [57] Zhirong Wu, Shuran Song, Aditya Khosla, Fisher Yu, Linguang Zhang, Xiaoou Tang, and Jianxiong Xiao. 3d shapenets: A deep representation for volumetric shapes. In *Proceedings of the IEEE conference on computer vision and pattern recognition*, pages 1912–1920, 2015. [5](#), [6](#), [7](#)
- [58] Saining Xie, Jiatao Gu, Demi Guo, Charles R Qi, Leonidas Guibas, and Or Litany. Pointcontrast: Unsupervised pre-training for 3d point cloud understanding. In *European conference on computer vision*, pages 574–591. Springer, 2020. [2](#), [6](#)
- [59] Le Xue, Mingfei Gao, Chen Xing, Roberto Martín-Martín, Jiajun Wu, Caiming Xiong, Ran Xu, Juan Carlos Niebles, and Silvio Savarese. Ulip: Learning a unified representation of language, images, and point clouds for 3d understanding. In *Proceedings of the IEEE/CVF Conference on Computer Vision and Pattern Recognition*, pages 1179–1189, 2023. [2](#), [3](#)
- [60] Li Yi, Vladimir G Kim, Duygu Ceylan, I-Chao Shen, Mengyan Yan, Hao Su, Cewu Lu, Qixing Huang, Alla Sheffer, and Leonidas Guibas. A scalable active framework for region annotation in 3d shape collections. *ACM Transactions on Graphics (ToG)*, 35(6):1–12, 2016. [5](#), [6](#), [7](#)
- [61] Xumin Yu, Lulu Tang, Yongming Rao, Tiejun Huang, Jie Zhou, and Jiwen Lu. Point-bert: Pre-training 3d point cloud transformers with masked point modeling. *arXiv preprint arXiv:2111.14819*, 2021. [5](#), [6](#)
- [62] Xumin Yu, Lulu Tang, Yongming Rao, Tiejun Huang, Jie Zhou, and Jiwen Lu. Point-bert: Pre-training 3d point cloud transformers with masked point modeling. In *Proceedings of the IEEE/CVF Conference on Computer Vision and Pattern Recognition*, pages 19313–19322, 2022. [1](#), [2](#), [3](#), [6](#)
- [63] Renrui Zhang, Ziyu Guo, Peng Gao, Rongyao Fang, Bin Zhao, Dong Wang, Yu Qiao, and Hongsheng Li. Point-m2ae: multi-scale masked autoencoders for hierarchical point cloud pre-training. *arXiv preprint arXiv:2205.14401*, 2022. [1](#), [2](#), [5](#), [6](#)
- [64] Zaiwei Zhang, Rohit Girdhar, Armand Joulin, and Ishan Misra. Self-supervised pretraining of 3d features on any point-cloud. In *Proceedings of the IEEE/CVF International Conference on Computer Vision*, pages 10252–10263, 2021. [2](#), [6](#)
- [65] Hengshuang Zhao, Li Jiang, Jiaya Jia, Philip HS Torr, and Vladlen Koltun. Point transformer. In *Proceedings of the IEEE/CVF International Conference on Computer Vision*, pages 16259–16268, 2021. [5](#)